

The periodic Anderson model from the atomic limit and FeSi

M. E. Foglio

*Instituto de Física “Gleb Wataghin”
Universidade Estadual de Campinas, UNICAMP
13083-970 Campinas, São Paulo, Brasil*

M. S. Figueira

*Instituto de Física, C.P. 100.093
Universidade Federal Fluminense, UFF
24001-970 Niterói, Rio de Janeiro, Brasil
(May 17, 2018)*

Abstract

The exact Green’s functions of the periodic Anderson model for $U \rightarrow \infty$ are formally expressed within the cumulant expansion in terms of an effective cumulant. Here we resort to a calculation in which this quantity is approximated by the value it takes for the exactly soluble atomic limit of the same model. In the Kondo region a spectral density is obtained that shows near the Fermi surface a structure with the properties of the Kondo peak. Approximate expressions are obtained for the static conductivity $\sigma(T)$ and magnetic susceptibility $\chi(T)$ of the PAM, and they are employed to fit the experimental values of FeSi, a compound that behaves like a Kondo insulator with both quantities vanishing rapidly for $T \rightarrow 0$. Assuming that the system is in the intermediate valence region, it was possible to find good agreement between theory and experiment for these two properties by employing the same set of parameters. It is shown that in the present model the hybridization is responsible for the relaxation mechanism of the conduction electrons.

71.28.+d, 71.27.+a, 75.20.Hr, 75.30.Mb

I. INTRODUCTION

In the present work we discuss approximate Green's Functions (GF) of the Periodic Anderson Model (PAM) that use the atomic limit as a starting point. We employ these GF to calculate the static magnetic susceptibility and the resistivity of FeSi.

FeSi has rather unusual magnetic properties,¹ and in particular a static susceptibility $\chi(T)$ that has a maximum $\chi(T_m)$ at about $T_m = 536$ K and vanishes for $T \rightarrow 0$ when the low temperature Curie tail is subtracted.² Several models were studied by Jacarino et.al.,¹ and they found that a simple one, with two very narrow rectangular bands separated by a gap, could be used to fit $\chi(T)$. The properties of FeSi are very similar to those of the Kondo insulators,²⁻⁴ and a very simple model that describes most of their properties would consist of two hybridized bands with two electrons,³ i.e.: an intrinsic semiconductor with an hybridization gap. Both $\chi(T)$ and the resistivity $\rho(T)$ of FeSi have activation laws with characteristic energies of order 0.1 eV, and although band structure calculations⁵ give comparable semiconducting gaps they can not reproduce the large values of $\chi(T)$. Also the measurements of infrared and optical reflectivity can not be described with the predictions of the band calculations,⁴ and the PAM seems a more adequate model, both because it becomes the previous model when the Coulomb repulsion between the localized electrons is neglected, i.e.: $U = 0$, and because the correlations present in the PAM could explain some of the observed features of FeSi.

A two-band Hubbard model⁶ has been already employed to study FeSi, and it is equal to the PAM when the dispersion in one band and the Coulomb repulsion in the other are zeroed. Another variant of the PAM was to add dispersion to the band of localized electrons, and this model has been studied both with $U \rightarrow \infty$ ⁷ and with finite U .⁸ It has been suggested³ that it would be interesting to describe the Kondo insulators employing the PAM with $U \rightarrow \infty$, and this approach is presented here to calculate both $\chi(T)$ and $\rho(T)$ employing approximate⁹ GF. This model has been also used to study the Kondo insulator $\text{Ce}_3\text{Bi}_4\text{Pt}_3$, employing the slave boson technique in the mean field approximation.^{10,11} Varma¹² argues that the strict Kondo lattice (i.e. with integer f occupation and therefore without charge fluctuations) is inappropriate for these systems, because it would be rather unlikely to find the chemical potential just in the hybridization gap, and that one would more likely find this situation in a mixed valence system. Our calculation shows that with the simplified model presented here, it is possible to give a fair description of the $\chi(T)$ and $\rho(T)$ of FeSi in a typical intermediate valence situation.¹³

In the study of solid state systems it is sometimes interesting to focus on the local states of the ions placed at the different sites of the crystal⁹. The space of the local or ionic states associated to a given site contains many states that are usually of little interest, generally because their occupation can be neglected at fairly low temperatures or frequencies when they are too far apart in energy from the ground state. It is then useful to eliminate these states from the model of the system, and the Hubbard operators^{14,15} are very convenient for that purpose. In the Anderson lattice we have a broad band of conduction electrons, identified by a subindex c , and the local d states, which will be identified with the subindex f for convenience. At each site j of the lattice there are four local states: the vacuum state $|j, 0\rangle$, the two states $|j, \sigma\rangle$ of one electron with spin component σ and the state $|j, 2\rangle$ with two local electrons. When $U \rightarrow \infty$ the state $|j, 2\rangle$ is empty, and one can use the Hubbard

operators to project it out from the space of local states at site j . One difficulty is that the usual expansions employed with the Fermi or Bose operators are not valid for these operators, and Hubbard introduced for his model of correlated electrons¹⁶ a diagrammatic expansion with cumulants¹⁷ which uses the electron hopping as a perturbation, and becomes the usual expansion when $U = 0$. The GFs employed in the present work are based on an extension¹⁸ of Hubbard's cumulant expansion that is valid for the Anderson lattice and uses the hybridization as perturbation; employing this expansion it is possible to express the exact GF in terms of an unknown effective cumulant^{9,19} $M_{2,\sigma}^{eff}(\omega)$. In this work we shall approximate the effective cumulant by $M_{2,\sigma}^{at}(z)$, which is obtained from the exact solution of the Anderson lattice in the atomic limit, namely when the band of uncorrelated electrons has zero width⁹. The spectral density obtained in this approximation, for typical values of the system parameters, shows a structure close to the chemical potential μ that corresponds to the Kondo resonance and affects the physical properties at low temperatures. This structure was absent from the GF derived from the cumulant expansion when only cumulants up to fourth order were employed^{18,20}, and this was the motivation to approximate the effective cumulant by a method that would include all the higher order cumulants that were absent in our previous calculations. Because of its atomic character, the approximate effective cumulant in our method is independent of the wave vector. Our GFs are therefore closely related to those employed by the dynamical mean field theory²¹ of the infinite dimensional problem,^{22,23} but rather than using a self consistency condition we use physical considerations to chose the parameters that define the effective cumulant. The dynamical mean field theory has been also employed to study the magnetism of the PAM²⁴ as well as the transfer of spectral weight in the spectroscopy of correlated electron systems described by this model.²⁵

Both the dynamical susceptibility and the conductivity require two-particle GFs in the theory of linear response, but we shall obtain approximate expressions of the static quantities employing the one-particle GFs introduced in this work. With these GF we obtain the total number of spin up and of spin down electrons in the presence of a weak magnetic field, and the static susceptibility $\chi(T)$ is then proportional to their difference divided into the magnetic field; we can then compare the ratio $\chi(T)/\chi(T_m)$ with the corresponding experimental value. To simplify the calculation of the effective cumulant we assume equal gyromagnetic factors g_f and g_c , although the extension to different g_f and g_c would not present essential difficulties.

It has been shown²⁶ that the limit $d = \infty$ can be used to give an approximate description of three-dimensional systems, and we shall then use an expression of $\sigma(T)$ that is valid in infinite dimension in our calculation for FeSi. This expression is derived from the well known Kubo formula, the vertex corrections cancel out when $d = \infty$,²⁷ and only the one-particle $G_{c,\sigma}(\mathbf{k}, z)$ are then necessary to calculate $\sigma(T)$. In this expression there are explicit sums over \mathbf{k} , but when nearest-neighbor hopping in a simple cubic lattice is considered, it is possible to derive expressions^{28,29} that depend on \mathbf{k} only through the unperturbed conduction electron energies $\varepsilon(\mathbf{k})$. As a further simplification that would not change the results in an essential way, we shall use a rectangular band with $-W \leq \varepsilon(\mathbf{k}) \leq W$.

Using the expressions of $\sigma(T)$ and $\chi(T)$ discussed above we fitted the experimental magnetic susceptibility¹ $\chi(T)/\chi(T_m)$ and the static resistivity² $\rho(T) = 1/\sigma(T)$ of FeSi with the same set of parameters in a typical situation of intermediate valence, obtaining a fairly reasonable agreement with the experimental values. To adjust the $\chi(T)$ at high T , it was necessary to assume that the thermal expansion affects the value of the system's parameters.

In Section II we discuss the Periodic Anderson Model (PAM) and the approximate one-particle GF employed in this work. In Section III we analyze the static magnetic susceptibility $\chi(T)$ and the static resistivity $\rho(T)$ of FeSi. Conclusions are presented in Section IV.

II. GREEN'S FUNCTIONS FOR THE PERIODIC ANDERSON MODEL

As discussed in Section I we employ Hubbard's operators.¹⁴ In the general case there is a fixed number n of orthogonal states $\{|j, a\rangle\}$ (identified by indices a) that span a space $\mathcal{E}_{j,n}$ at each site j , where $j = 1, 2, \dots, N_s$ and N_s is the number of sites. To each site j we associate the n^2 Hubbard operators

$$X_{j,ab} = |j, a\rangle \langle j, b| \quad , \quad (2.1)$$

which transform the state $|j, b\rangle$ into the state $|j, a\rangle$, i.e. $X_{j,ab}|j, b\rangle = |j, a\rangle$. The product rules for two operators at the same site are given by

$$X_{j,ab} X_{j,cd} = \delta_{b,c} X_{j,ad} \quad , \quad (2.2)$$

and we chose properties equivalent to those of the usual Fermi or Bose operators when they are at different sites. We then say that $X_{j,ab}$ is of the ‘‘Fermi type’’ (‘‘Bose type’’) when the number of electrons in the two states $|j, a\rangle$ and $|j, b\rangle$ differ by an odd (even) number. For $j \neq j'$ we then use $\{X_{j,ab}, X_{j',cd}\} = 0$ when the two operators are of the ‘‘Fermi type’’ and $[X_{j,ab}, X_{j',cd}] = 0$ when at least one is of the ‘‘Bose type’’ (as usual³⁰ $[a, b] = ab - ba$ and $\{a, b\} = ab + ba$).

A. The Anderson lattice for $U \rightarrow \infty$

The Anderson lattice with finite U is described by the Hamiltonian

$$H = \sum_{\mathbf{k}\sigma} E_{\mathbf{k},\sigma} C_{\mathbf{k}\sigma}^\dagger C_{\mathbf{k}\sigma} + \sum_{j\sigma} E_{j,\sigma} f_{j\sigma}^\dagger f_{j\sigma} + \sum_j U f_{j\sigma}^\dagger f_{j\sigma} f_{j\bar{\sigma}}^\dagger f_{j\bar{\sigma}} + \sum_{jk\sigma} \left(V_{j,\mathbf{k},\sigma} f_{j\sigma}^\dagger C_{\mathbf{k}\sigma} + H.C. \right) \quad , \quad (2.3)$$

where $C_{\mathbf{k}\sigma}^\dagger$ ($C_{\mathbf{k}\sigma}$) is the usual creation (annihilation) operator of conduction band electrons with wavevector \mathbf{k} and spin component $\sigma\hbar/2$, where $\sigma = \pm 1$. The $f_{j\sigma}^\dagger$ and $f_{j\sigma}$ correspond to the local f or d electrons at site j , and

$$V_{j,\mathbf{k},\sigma} = V(k) \exp(i\mathbf{k} \cdot \mathbf{R}_j) \quad . \quad (2.4)$$

When $U = 0$ Eq.(2.3) describes two hybridized bands of uncorrelated electrons.

The state space of the f-electrons at each site j is spanned by the four states $|j, 0\rangle$, $|j, \sigma\rangle$ and $|j, 2\rangle$, with $\sigma = \pm 1$. The state $|j, 2\rangle$ is empty when $U \rightarrow \infty$, and we shall consider a reduced space of states by projecting $|j, 2\rangle$ out, so that $\mathcal{E}_{j,n}$ is a three dimensional space. To make the connection with the Hubbard operators one could substitute the identity³¹

$$f_{j\sigma} = X_{j,0\sigma} + \sigma X_{j,\bar{\sigma}d} \quad (2.5)$$

into Eq. (2.3), where the factor σ is necessary to obtain the correct phase of the states. Eliminating the $X_{j,\bar{\sigma}d}$ and $X_{j,22}$ one obtains the projection of H into the reduced space, namely

$$H_r = \sum_{\mathbf{k}\sigma} E_{\mathbf{k},\sigma} C_{\mathbf{k},\sigma}^\dagger C_{\mathbf{k},\sigma} + \sum_{j,\sigma} E_{j,\sigma} X_{j,\sigma\sigma} + \sum_{j\mathbf{k}\sigma} \left(V_{j,\mathbf{k},\sigma} X_{j,0\sigma}^\dagger C_{\mathbf{k},\sigma} + V_{j,\mathbf{k},\sigma}^* C_{\mathbf{k},\sigma}^\dagger X_{j,0\sigma} \right) \quad . \quad (2.6)$$

1. The cumulant expansion

The cumulant expansion has been employed by several authors to study Ising's and Heisenberg's models,³² while Hubbard¹⁷ extended the method to a quantum problem with fermions. In this technique the cumulant averages³³ are used to rearrange the usual perturbative expansion,¹⁷ and it is possible to derive a diagrammatic expansion involving unrestricted lattice sums of connected diagrams, that satisfies a linked cluster theorem. This technique was extended to the Anderson lattice,¹⁸ and a brief description is given here. The method employs the Grand Canonical Ensemble of electrons, and it is then convenient to introduce

$$\mathcal{H} = H - \mu \left\{ \sum_{\vec{k},\sigma} C_{\vec{k},\sigma}^\dagger C_{\vec{k},\sigma} + \sum_{ja} \nu_a X_{j,aa} \right\} \quad , \quad (2.7)$$

where μ is the chemical potential and ν_a is the number of electrons in the state $|j, a\rangle$. The last term in Eq. (2.6) will be considered as the perturbation, and the exact and unperturbed averages of any operator A are respectively denoted by $\langle A \rangle_{\mathcal{H}}$ and $\langle A \rangle$. It is also convenient to introduce

$$\varepsilon_{j,a} = E_{j,a} - \mu \nu_a \quad (2.8)$$

$$\varepsilon_{\mathbf{k}\sigma} = E_{\mathbf{k}\sigma} - \mu \quad , \quad (2.9)$$

because these are the forms that consistently appear in the calculations.

The Matsubara expansion³⁰ is employed, so that τ is an imaginary time in the GFs $\left\langle \left(\widehat{X}_{j,\alpha}(\tau) \widehat{X}_{j',\alpha'}(\tau') \right)_+ \right\rangle_{\mathcal{H}}$, where $\alpha \equiv (a, b)$ identifies the transition $b \rightarrow a$, and

$$\widehat{X}_{j,\alpha}(\tau) = \exp(\tau\mathcal{H}) X_{j,\alpha} \exp(-\tau\mathcal{H}) \quad . \quad (2.10)$$

The subindex $+$ in the definition of the GF indicates that the operators inside the parenthesis are taken in the order of increasing τ to the left, with a change of sign when two Fermi-type operators have to be exchanged to obtain this ordering. The inverse of Plank's \hbar and of Boltzmann's k_B are usually included into the real and imaginary temperatures T and τ , as well as in several other parameters, so that all of them are given in terms of a common energy unit.

Some of the infinite diagrams which contribute to the GF $\left\langle \left(\widehat{X}_{j,\alpha}(\tau) \widehat{X}_{j',\alpha'}(\tau') \right)_+ \right\rangle_{\mathcal{H}}$ are shown in figure 1, and the full circles (f-vertices) correspond to the cumulants of the f-electrons. Each line reaching a vertex is associated to one of the X operators of the cumulant, and the free lines (i.e. those that do not join an empty circle) correspond to the external X operators appearing in the exact GF. An explicit definition of the cumulants can be found in the references 17,18,34, and they can be calculated by employing a generalized Wick's theorem.^{34–36}

The first diagram in figure 1a corresponds to the simplest free propagator $\left\langle (X_{j,\alpha}(\tau) X_{j',\alpha'}(\tau'))_+ \right\rangle$, and the second diagram in that figure has an empty circle (c-vertex) that corresponds to the conduction electron cumulant, equal to the free propagator $\left\langle \left(C_{k\sigma}(\tau) C_{k\sigma}^\dagger(\tau') \right)_+ \right\rangle \equiv G_{c,\sigma}^o(\mathbf{k},\tau)$. The interaction is represented by the lines (edges) joining two vertices and, because of the structure of the hybridization, they always join a c-vertex to an f-vertex; the number of edges in a diagram gives its order in the perturbation expansion.

Cumulants containing statistically independent operators are zero, and those appearing in the present formalism (with the hybridization as perturbation) vanish unless they contain only X operators at the same site or only C or C^\dagger operators with the same k and σ . The only non-zero c-cumulants are of second order, because the uncorrelated c-operators satisfy Wick's theorem. On the other hand, the f-vertices can have many legs, all corresponding to X operators at the same site, like the fourth and sixth order cumulants appearing in the rather more complicated diagram shown in figure 1c.

All the infinite diagrams that contribute to the GF with cumulants of at most second order are shown in figure 1a, and this family is the “chain approximation” (CHA), which gives the exact solution of Eq. (2.3) when there is no Coulomb correlation ($U = 0$). When the spin is eliminated from the problem, the Hamiltonian of equation (2.6) corresponds to a system of two hybridized bands without any Coulomb repulsion (there can be only one or zero f-electrons at each site), and the CHA is again an exact solution.¹⁸ The diagrams of the c-electron propagator in the same approximation are shown in figure 1b.

In the Feynmann perturbation expansion, Wick's theorem is valid and only second order propagators appear, while the interactions are provided by the Coulomb interaction. In the present treatment, the U disappears in the limit $U \rightarrow \infty$ (or is included in the unperturbed Hamiltonian when U is finite), and the correlations appear through the non-zero cumulants of X operators with order greater than two, which include propagators of two or more particles. In the Feynmann expansion of the one particle GF, the two particle GF appear in the self-energy, which contains all the correlations.

2. The spectral density of the GF and the occupation number

In the Anderson lattice with $U \rightarrow \infty$ one can introduce one-particle GFs of local electrons

$$\left\langle (X_{j,0\sigma}(\tau) X_{j',\sigma 0}(\tau'))_+ \right\rangle_{\mathcal{H}}, \quad (2.11)$$

as well as GFs for the c-electrons $\left\langle \left(C_{k\sigma}(\tau) C_{k'\sigma}^\dagger(\tau') \right)_+ \right\rangle_{\mathcal{H}}$ and “crossed” GFs of the type $\left\langle \left(X_{j,0\sigma}(\tau) C_{k'\sigma}^\dagger(\tau') \right)_+ \right\rangle_{\mathcal{H}}$, all of them defined in the intervals $0 \leq \tau, \tau' \leq \beta \equiv 1/T$. It is possible to associate a Fourier series to these GFs because of their boundary condition in this variable,¹⁸ and the coefficients correspond to the Matsubara frequencies $\omega_\nu = \pi\nu/\beta$ (where ν are all the positive and negative odd integer numbers). One can also transform the GF to reciprocal space¹⁸ so that

$$\left\langle \left(X_{j,0\sigma}(\tau) X_{j',\sigma 0}(\tau') \right)_+ \right\rangle_{\mathcal{H}} = \frac{1}{\beta N_s} \sum_{\mathbf{k}, \mathbf{k}'} \sum_{\omega_\nu, \omega_{\nu'}} \exp \left[i \left(\mathbf{k} \cdot \mathbf{R}_j - \mathbf{k}' \cdot \mathbf{R}_{j'} - i(\omega_\nu \tau + \omega_{\nu'} \tau') \right) \right] \left\langle \left(X_{\mathbf{k},0\sigma}(\omega_\nu) X_{\mathbf{k}',\sigma 0}(\omega_{\nu'}) \right)_+ \right\rangle_{\mathcal{H}} \quad , \quad (2.12)$$

and because of the invariance against time and lattice translations^{18,37}

$$\left\langle \left(X_{\mathbf{k},0\sigma}(\omega_\nu) X_{\mathbf{k}',\sigma 0}(\omega_{\nu'}) \right)_+ \right\rangle_{\mathcal{H}} = G_{ff,\sigma}(\mathbf{k}, \omega_\nu) \delta_{\mathbf{k}', \mathbf{k}} \delta_{\nu+\nu', 0} \quad , \quad (2.13)$$

where $\delta_{\mathbf{k}', \mathbf{k}}$ and $\delta_{\nu+\nu', 0}$ are Kronecker’s deltas, because the \mathbf{k} and ω_ν are discrete variables. Transforming the eigenstates of the c-electrons to the Wannier representation, one obtains the equivalent relations for $G_{cc,\sigma}(\mathbf{k}, \omega_\nu)$ and $G_{fc,\sigma}(\mathbf{k}, \omega_\nu)$. Considering that the coefficients of the τ Fourier series for each \mathbf{k} are the values of a function of the complex variable $z = \omega + iy$ at the points $z_\nu = i \omega_\nu$, it is possible to make the analytic continuation to the upper and lower half-planes of z in the usual way,³⁸ obtaining, e.g. from the $G_{ff,\sigma}(\mathbf{k}, \omega_\nu)$, a function $G_{ff,\sigma}(\mathbf{k}, z)$ which is minus the Fourier transform of the double time GF.³⁹

If we assume the system to be uniform, the occupation of the local state $\langle X_{j,\sigma\sigma} \rangle$ does not depend on j , and it is given by

$$n_{f,\sigma} = \int_{-\infty}^{\infty} \rho_{f,0\sigma}(\omega) f_T(\omega) d\omega \quad , \quad (2.14)$$

where

$$f_T(z) = [1 + \exp(\beta z)]^{-1} \quad (2.15)$$

is the Fermi function and

$$\rho_{f,0\sigma}(\omega) = \frac{1}{\pi} \lim_{\eta \rightarrow 0} \text{Im} \left\{ \frac{1}{N_s} \sum_{\mathbf{k}} G_{ff,\sigma}(\mathbf{k}, \omega + i|\eta|) \right\} \quad (2.16)$$

is the spectral density associated to the transition $\sigma \rightarrow 0$, abbreviated with $(0, \sigma)$. Using the same $\rho_{f,0\sigma}(\omega)$ it is also possible to obtain the occupation $\langle X_{j,00} \rangle = n_{f,0}$ of the empty state $|0\rangle$, namely

$$n_{f,0} = \int_{-\infty}^{\infty} \rho_{f,0\sigma}(\omega) (1 - f_T(\omega)) d\omega \quad . \quad (2.17)$$

All the corresponding quantities for the conduction electrons are obtained by replacing $G_{cc,\sigma}(\mathbf{k}, z)$ for $G_{ff,\sigma}(\mathbf{k}, z)$.

The f-electron GF is given in the CHA (cf. the diagrams in figure 1a) by

$$G_{ff,\sigma}(\mathbf{k}, z) = -\frac{D_{\sigma}^0(z - \varepsilon_{\mathbf{k}\sigma})}{(z - \varepsilon_{1,\sigma}(\mathbf{k}))(z - \varepsilon_{2,\sigma}(\mathbf{k}))} \quad , \quad (2.18)$$

where the energies $\varepsilon_{1,\sigma}(\mathbf{k})$ and $\varepsilon_{2,\sigma}(\mathbf{k})$ are the two elementary excitations with wave vector \mathbf{k} and spin component σ , resulting from the hybridization of a band $\varepsilon_{\mathbf{k}\sigma}$ and a dispersionless band of energy $\varepsilon_f = E_{j\sigma} - \mu$, with a reduced hybridization constant $\sqrt{D_{\sigma}}V(k)$. These energies are given by the two roots of $(z - \varepsilon_f)(z - \varepsilon_{\mathbf{k}\sigma}) - D_{\sigma}|V(k)|^2 = 0$, where

$$D_{\sigma} = \int_{-\infty}^{\infty} \rho_{f,0\sigma}(\omega) d\omega = \langle X_{00} + X_{\sigma\sigma} \rangle \quad . \quad (2.19)$$

The spectral density for the unperturbed f-electrons is a δ -function at ε_f , and $\rho_{f,0\sigma}(\omega)$ becomes two bands with a gap centered at ε_f and roughly proportional to the reduced hybridization constant $\sqrt{D_{\sigma}}V$ in the CHA. When the system is in the “Kondo region” in which the local state has nearly the maximum occupation compatible with the paramagnetic state, viz. $n_{f,\sigma} = 0.5$ in the average, a narrow temperature-dependent peak, the “Kondo peak”, should appear very close to the chemical potential, i.e. near to $\omega = 0$ in the variables we use. This peak is responsible for many properties of the “heavy fermions”,⁴⁰ and it is closely related to the increase in resistivity when T decreases, observed in many metals with magnetic impurities at low T. In combination with the effect of phonons, that make the resistivity increase with T, it is responsible for the minimum in resistivity, named the Kondo effect, that is observed in those systems. To explain this behavior it was essential to consider a third order perturbation that includes spin-flip processes.⁴¹ These processes are absent from the CHA, because diagrams with only second order cumulants do not include them, so that the absence of the Kondo peak in that approximation is not surprising. The GFs proposed in this work avoid the laborious explicit calculation of higher order cumulants by including all of them in an approximate way.

3. The exact Green's functions

In the calculation with the usual Fermi or Bose operators, the one-particle propagator of the f-electron is given by a sum of diagrams of the same type⁴² shown in figure 1a but with each vertex corresponding to the sum of all “proper” (or irreducible) diagrams.^{30,43} The same result is found in the cumulant expansion of the Hubbard model for $d \rightarrow \infty$,^{19,44} when the electron hopping is employed as perturbation. The vertices then represent an “effective cumulant” $M_{2,\sigma}^{eff}(z)$, that is independent of \mathbf{k} because only diagrams of a special type contribute to this quantity for $d \rightarrow \infty$.

In the cumulant expansion of the Anderson lattice¹⁸ we employ the hybridization rather than the hopping as a perturbation, and the exact solution of the conduction electrons problem in the absence of hybridization is part of the zeroth order Hamiltonian. For this reason it became necessary to extend Metzner’s derivation¹⁹ to the Anderson lattice, and we have shown⁴⁵ that the same type of results obtained by Metzner are also valid for this model. These results had been used⁹ to obtain the exact GF employed in the present work, but since then we realized that the expression of the exact GF is valid for all dimensions and it is not

necessary to assume infinite dimension in that part of the derivation. As with the Feynmann diagrams, one can rearrange all those that contribute to the exact $G_{ff,\sigma}(\mathbf{k}, z)$ by defining an effective cumulant $M_{2,\sigma}^{eff}(\mathbf{k}, z)$, that is given by all the diagrams of $G_{ff,\sigma}(\mathbf{k}, z)$ that can not be separated by cutting a single edge (usually called “proper” or “irreducible” diagrams). The exact GF $G_{ff,\sigma}(\mathbf{k}, z)$ is then given by the family of diagrams in figure 1a, but with the effective cumulant $M_{2,\sigma}^{eff}(\mathbf{k}, z)$ in place of the bare cumulant $M_{2,\sigma}^0(z) = -D_\sigma^0/(z - \varepsilon_f)$ at all the filled vertices. The exact GF for the f electron is then written as

$$G_{ff,\sigma}(\mathbf{k}, z) = M_{2,\sigma}^{eff}(\mathbf{k}, z) \frac{1}{1 - |V(\mathbf{k})|^2 G_{c,\sigma}^o(\mathbf{k}, z) M_{2,\sigma}^{eff}(\mathbf{k}, z)}, \quad (2.20)$$

where $G_{c,\sigma}^o(\mathbf{k}, z) = -1/(z - \varepsilon(\mathbf{k}))$ is the frequency Fourier transform of $G_{c,\sigma}^o(\mathbf{k}, \tau)$, and in a similar way one obtains the exact GF for the c-electron, namely

$$G_{cc,\sigma}(\mathbf{k}, z) = \frac{-1}{z - \varepsilon(\mathbf{k}) + |V(\mathbf{k})|^2 M_{2,\sigma}^{eff}(\mathbf{k}, z)}. \quad (2.21)$$

It is clear that for arbitrary dimension we have not gained much with Eq.(2.20), because the calculation of $M_{2,\sigma}^{eff}(\mathbf{k}, z)$ is as difficult as that of $G_{ff,\sigma}(\mathbf{k}, z)$. We circumvent this obstacle by resorting to replace $M_{2,\sigma}^{eff}(\mathbf{k}, z)$ by the corresponding quantity $M_{2,\sigma}^{at}(z)$ of an exactly soluble model, which is the atomic limit of the Anderson lattice. The hopping is neglected in this system, described by the Hamiltonian of Eqs. (2.3) or (2.6) with $E_{\mathbf{k},\sigma} = E_0$, and it already contains the basic physics of the formation of the singlet ground state and of the appearance of the Kondo peak in the PAM, as it is discussed in review articles.⁴⁶ Because of its atomic character, the approximate effective cumulant $M_{2,\sigma}^{at}(z)$ thus obtained is independent of \mathbf{k} , and can be calculated exactly as shown in the next section. Being a special case of the PAM, it implicitly contains all the higher order cumulants.

The effective cumulant is also independent of \mathbf{k} when $d \rightarrow \infty$, and the very successful “dynamical mean field theory”²¹ also employs GFs corresponding to those in Eqs. (2.20,2.21).

B. The exact solution in the atomic limit

The exact solution of the local problem has been already used in different ways to study the Anderson lattice. The limit $U \rightarrow \infty$ was studied in the intermediate valence case⁴⁷ by considering only the lowest four eigenstates of the local Hamiltonian and the magnetic instabilities and susceptibility were discussed employing the resulting self-consistent Hamiltonian.⁴⁸ Considering only the atomic limit, viz. taking $E_{\mathbf{k},\sigma} = E_0^a$, Alascio et.al.^{49,50} studied the model for the whole range of parameters, showing that “most of the essential characteristics” of these systems “are present in this crudely simplified Hamiltonian”. Simões et.al.⁵¹ employed the atomic limit together with a diagrammatic method,⁵² that is essentially equivalent to our CHA, considering both the hopping and the hybridization as perturbations. An important improvement of the technique was to apply the same diagrammatic expansion to the exact solution of the atomic limit,^{53,54} employing only the hopping as perturbation, and this technique has also been applied to study the problem with finite U .^{55,56}

As discussed in the previous section we introduce the exact expression for the GF that is given in terms of an effective cumulant $M_{2,\sigma}^{eff}(\mathbf{k}, z)$, however replacing this quantity by the approximate $M_{2,\sigma}^{at}(z)$. As this treatment was derived from the diagrammatic expansion¹⁸ which uses the hybridization as perturbation and employs the exact solution of the uncorrelated conduction band, it seems a better starting point than considering the hopping as a perturbation, because the hybridization is usually rather smaller than the bandwidth. The atomic limit has also been employed, within the framework of the dynamical mean field theory, to study the transport properties of the symmetric PAM.⁵⁷

1. The exact GF in the atomic limit

Taking $E_{\mathbf{k},\sigma} = E_0^a$ and introducing a local hybridization $V_{j,\mathbf{k},\sigma} = V_{j,\sigma}$, the eigenvalue problem of Eqs. (2.3) or (2.6) has an exact solution,⁴⁷ and the GFs can be calculated analytically. As the problem is fully local, one can use the Wannier representation for the creation and annihilation operators $C_{j,\sigma}^\dagger$ and $C_{j,\sigma}$ of the c-electrons, and write $H_r = \sum_j H_j$, where H_j is the local Hamiltonian

$$H_j = \sum_{\sigma} \left\{ E_0^a C_{j,\sigma}^\dagger C_{j,\sigma} + E_{j,\sigma} X_{j,\sigma\sigma} + \left(V_{j,\sigma} X_{j,0\sigma}^\dagger C_{j,\sigma} + V_{j,\sigma}^* C_{j,\sigma}^\dagger X_{j,0\sigma} \right) \right\} \quad , \quad (2.22)$$

and the subindex j can be dropped because we assume a uniform system.

We shall denote with $|n, r\rangle$ the eigenstates of the Hamiltonian H_j with eigenvalues $E_{n,r}$, where n is the total number of electrons in that state, and r characterizes the different states. These eigenstates satisfy

$$\mathcal{H} |n, r\rangle = \varepsilon_{n,r} |n, r\rangle \quad , \quad (2.23)$$

where \mathcal{H} is given in Eq. (2.7) and $\varepsilon_{n,r} = E_{n,r} - n\mu$ (cf. Eq. (2.8)). In Table I we give the properties of the $|n, r\rangle$ states: number of electrons n , name of the state r , z component of spin S_z and $\varepsilon_{n,r} = E_{n,r} - n\mu$. The twelve eigenvalues $\varepsilon_{n,r}$ of \mathcal{H}_j are represented in figure 2, and those corresponding to different occupations $n = 0, 1, 2, 3$ are drawn in different columns. The states are identified in the figure by the numbers r above the levels, and the lines joining different levels correspond to the possible transitions that contribute to the GF.

It is now straightforward to express the Fourier transform of the f-electron GF in the form

$$\left\langle \left(\widehat{X}_{j,0\sigma}(\omega_s) \widehat{X}_{j,0\sigma}^\dagger(\omega'_s) \right)_+ \right\rangle_{\mathcal{H}} = \Delta(\omega_s + \omega'_s) G_{ff,0\sigma}^{at}(\omega_s) \quad , \quad (2.24)$$

where

$$G_{ff,0\sigma}^{at}(\omega_s) = -e^{\beta\Omega} \sum_{n,r,r'} \frac{\exp(-\beta\varepsilon_{n,r}) + \exp(-\beta\varepsilon_{n-1,r'})}{i\omega_s + \varepsilon_{n-1,r'} - \varepsilon_{n,r}} \left| \langle n-1, r' | X_{0\sigma} | n, r \rangle \right|^2 \quad (2.25)$$

and $\Omega = -kT \ln \sum \exp(-\beta\varepsilon_{n,r})$ is the grand canonical potential.⁵⁸ The equivalent equations for the c-electrons are obtained by just replacing $\left| \langle n-1, r' | X_{0\sigma} | n, r \rangle \right|^2$ in Eq. (2.25) by $\left| \langle n-1, r' | C_{j,\sigma} | n, r \rangle \right|^2$.

The f-electron GF can be written in the form

$$G_{ff,0\sigma}^{at}(\omega_s) = -\exp(\beta\Omega) \sum_{j=1}^8 \frac{m_j}{i\omega_s - u_j} \quad , \quad (2.26)$$

where u_j are the poles and m_j the residues of the GF. There are only eight different u_j for the f-electron GF, because different transitions have the same energy and the residues of some transitions are zero. Each $u_j = -(\varepsilon_{n-1,r'} - \varepsilon_{n,r})$ corresponds to the lines identified with j that appear joining the levels in figure 2, the two lines u_1 and the single lines u_3 and u_7 represent transitions that are allowed in the absence of hybridization, while the remaining ones correspond to transitions that are forbidden in that limit. It is important to notice that for a system with given values of E_0^a , E_f and V , the position of the levels in figure 2 changes with the chemical potential μ . In that figure we have $E_0^a = \mu$ and $E_f < E_0^a = \mu$, and in that system the ground state is always the singlet $|2,9\rangle$, which has no magnetic moment in the absence of field but can have a rather large induced moment because of the proximity of the magnetic triplet.⁵⁰

C. The atomic effective cumulant approximation

The atomic effective cumulant approximation (AECA) consists in substituting $M_{2,\sigma}^{eff}(z)$ in Eq. (2.20) by an approximate $M_{2,\sigma}^{at}(z)$ derived from the exact solution of the atomic limit, obtained by solving for $M_{2,\sigma}^{at}(z)$ in the equation that is the atomic equivalent of Eq. (2.20). One then obtains

$$M_{2,\sigma}^{at}(z) = \frac{(z - E_0^a + \mu) G_{ff,0\sigma}^{at}(z)}{(z - E_0^a + \mu) - |V|^2 G_{ff,0\sigma}^{at}(z)} \quad , \quad (2.27)$$

and from the point of view of the cumulant expansion, it contains all the irreducible diagrams that contribute to the exact $M_{2,\sigma}^{eff}(z)$. It should be emphasized that this diagrams contain loops of any size, because there is no excluded site in this expansion, and all the filled circles correspond to the same site, although they appear as different vertices in the diagram. The difference between the exact and approximate quantities is that different energies $E_{\mathbf{k},\sigma}$ appear in the c-electron propagators of the effective cumulant $M_{2,\sigma}^{eff}(z)$, while these energies are all equal to E_0^a in $M_{2,\sigma}^{at}(z)$. Although $M_{2,\sigma}^{at}(z)$ is for that reason only an approximation, it contains all the diagrams that should be present, and one would expect that the corresponding GF would have fairly realistic features.

One still has to decide what value of E_0^a should be taken. As the most important region of the conduction electrons is the Fermi energy, we shall use $E_0^a = \mu - \delta E_0$, leaving the freedom of small changes δE_0 to adjust the results to particular situations, but fixing its value for a given system when μ has to change to keep the total number of electrons N_t fixed, as for example when changing the temperature T .

Another important point, is that concentrating all the conduction electrons at E_0^a would overestimate their contribution to the effective cumulant, and we shall then reduce the hybridization by a coefficient that gives the fraction of c-electrons which contribute most. We consider that this is of the order of $V\rho^0$, where ρ^0 is the density of states of the free

c electrons per site and per spin, and to be more definite we chose $\pi V \rho^0$, so the effective hybridization constant V_a coincides with the usual “mixing strength” $\Delta = \pi V^2 \rho^0$. This is essentially the same choice made by Alascio et.al.⁴⁹ in their localized description of valence fluctuations. Note that V_a is only used in the calculation of $M_{2,\sigma}^{at}(z)$, and that the full value must be substituted in the V that appears explicitly in Eq. (2.20), because the whole band of conduction energies is used in $G_{c,\sigma}^o(\vec{k}, z) = -1/(z - \varepsilon_{\mathbf{k}\sigma})$.

The spectral density $\rho_f \equiv \rho_{f,0\sigma}(\omega)$ for several values of T is shown in figure 3 assuming the following system’s parameters: $E_{j,\sigma} = E_f = -0.5$, $\mu = 0.$, a local hybridization $V = 0.3$ and a density of states of the unperturbed band electrons given by a rectangular band of width π centered at the origin. As discussed before, we include adequate universal constants into the different parameters, so that all of them are expressed in terms of a single energy taken as unit. In the present case we can take that unit to be equal to the total width of the band divided into π .

The localized energy E_f of the local state is well below the Fermi surface in this figure, corresponding to a typical Kondo region. The spectral density ρ_f does not change with T below a certain value, which is approximately $T = 10^{-3}$ in figure 3, because below this T the state $|n = 2, r = 9\rangle$ is the only occupied in the atomic limit and therefore $M_{2,\sigma}^{at}(z)$ does not change by further decreasing T . Other states are occupied at higher T , and the changes in $M_{2,\sigma}^{at}(z)$ are reflected in ρ_f . The ρ_f obtained by the AECA at the lowest T in the figure is basically the same ρ_f of the CHA in the region close to $\varepsilon_f = -0.5$, but it has also a structure close to the Fermi surface (i.e. at $\omega = 0$) that is absent in the CHA. The spectral density in this region has the main characteristics of the Kondo peak, namely its localization and the decrease of its intensity when T increases, as can be seen in figure 3. This structure shows a pseudo gap, as was obtained using other methods,^{59,60} but with a peak below the Fermi energy that is not as sharp and that becomes more complex with increasing T , an effect that we believe is due to the use of the atomic model to estimate $M_{2,\sigma}^{eff}(z)$.

In figure 4 it is plotted the dependence of the spectral density with μ showing a main structure that follows ε_f , and a smaller one, corresponding to the Kondo peak, that remains fixed at the Fermi surface when the system remains in the Kondo region, i.e. when $\varepsilon_f < 0$. When ε_f approaches the Fermi surface in the intermediate valence region the two parts of the spectrum merge, and a single structure then follows ε_f for $\varepsilon_f > 0$.

The AECA gives a ρ_f that roughly agrees with the results obtained by other methods,⁵⁹ but the details of the spectral density near the Kondo resonance depend in a very delicate way on the behavior of $M_{2,\sigma}^{eff}(z)$ near that region. In the calculation of $M_{2,\sigma}^{at}(z)$ all the band structure is replaced by a single value E_0^a , and it is therefore not surprising that the AECA results are less precise than those of reference,⁵⁹ which uses the decoupling of the equations of motion followed by the self-consistent determination of the averages resulting from that procedure. This last method, as well as the dynamical mean field theory,⁴⁰ require some heavy computation while the AECA is fairly simple from that point of view. As the spectral density ρ_f in the AECA has the same overall behavior shown by the methods mentioned above, it can be used to obtain rather reasonable values of many physical properties and of their dependence with T and other parameters. The main interest in this method, is that it is very natural to make the extension to more complex systems with numerous local states, that can be simplified by using the Hubbard operators to project the Hamiltonian to the

subspace of states of interest. The use of the AECA would then make it possible to calculate properties of those systems without employing too heavy computation.

III. MAGNETIC SUSCEPTIBILITY AND RESISTIVITY OF FESI

We discuss here the Kondo insulators within the context of the PAM, employing the approximate GF introduced in Section II C. We consider the extreme case of $U \rightarrow \infty$, and apply it to FeSi, which seems to behave like a typical Kondo insulator.²⁻⁴ Although this compound should be better described with a finite U , we believe that this would not change too much the basic properties from the ones presented here, but there would certainly be changes in the parameters necessary to reproduce the measured properties of FeSi when a finite U is employed. Both the static conductivity $\sigma(T)$ and magnetic susceptibility $\chi(T)$ vanish when $T \rightarrow 0$, and we can describe this dependence of the two properties, as well as their initial rapid increase and posterior behavior for increasing T , with the same set of values of our model's parameters. The agreement with $\chi(T)$ is very good at not too high T , but to obtain a good agreement at high T one should consider that the parameters are affected by thermal expansion in this region.

To select the total number n_{tot} of electrons per site for our model we first considered that in a band calculation of FeSi,⁵ where all the Fe $3d^7 4s^1$ and Si $3s^2 3p^2$ states were treated as valence electrons, the corresponding 48 valence electrons per unit cell (4FeSi) completely filled the lowest 24 valence bands. To make a connection with the much simpler PAM, we first notice that a model of two hybridized bands with two electrons per site would also fill the lowest band, and that this model was considered to be a good starting point to describe FeSi.³ Therefore it seemed that $n_{tot} = 2$ would be a good choice for our model. It is easier to keep a constant μ to calculate the T dependence of properties, but the corresponding changes in n_{tot} where large enough to produce substantial changes in $\chi(T)$ but minor changes in $\rho(T)$ as the temperature increases. It was then necessary to resort to the more laborious calculation at constant n_{tot} .

The parameters employed in the numerical calculations are numbers that have to be scaled later to describe the different particular physical situations, and for brevity we shall call them “unscaled parameters”. This unscaled parameters are usually chosen so that one physical magnitude, like the band width, is equal to one. In our case we use a rectangular band, but fix the unscaled total width $2W = 5\pi$, this value (or any other of similar order of magnitude) being convenient from the point of view of the numerical calculation. The unscaled energy parameters can then be considered to be given in units of $2W/5\pi$. In this paper we shall present a study of a typical intermediate valence situation with $n_{tot} = 2$, and these two conditions are satisfied by employing values of $E_{f,\sigma}$ and μ close to 4. when $2W = 5\pi$. We shall then use as parameter the common value E_f of $E_{f,\sigma}$ in the absence of magnetic field, and fix an unscaled value of $E_f = 4$. As a final step, the value of μ that satisfies $n_{tot} = 2$ has to be obtained before the $\chi(T)$ and $\rho(T)$ are calculated.

When $U \rightarrow \infty$, the average of the identity in the space of the local states at site j

$$X_{j;\uparrow\uparrow} + X_{j;\downarrow\downarrow} + X_{j;00} = I_j \quad , \quad (3.1)$$

gives the “completeness” condition

$$n_{f,\uparrow} + n_{f,\downarrow} + n_{f,0} = 1 \quad , \quad (3.2)$$

where $n_{f,\sigma}$ and $n_{f,0}$ are the average occupation number per site of f-electrons states $|j, \sigma\rangle$ and $|j, 0\rangle$ respectively. This relation gives the conservation of probability of the local states at site j , and it is clear that it should be satisfied before most properties of the system could be calculated. The equivalent condition for the uncorrelated conduction electrons, obtained from the identity $C_{j,\sigma}^\dagger C_{j,\sigma} + C_{j,\sigma} C_{j,\sigma}^\dagger = 1$, is satisfied for each σ in all the approximations that we have employed for the cumulant expansion, but the Eq. (3.2) is not satisfied for the local electrons in the $U \rightarrow \infty$ limit.¹⁸ The origin of this problem has been already discussed,⁶¹ and an exact solution for some families of diagrams, together with a conjecture for the general case, has been presented,³⁷ but this treatment is not adequate for the approximate GF we employ in this work. We have then applied an ‘‘ad hoc’’ renormalization, multiplying each unrenormalized $G_{ff,\sigma}^u(\mathbf{k}, z)$ by a constant x_σ , so that the occupation numbers calculated with the renormalized $G_{ff,\sigma}(\mathbf{k}, z) = x_\sigma G_{ff,\sigma}^u(\mathbf{k}, z)$ satisfy Eq.(3.2). The two GF with $\sigma = \pm 1$ are equal in the absence of magnetic field, so that Eq.(3.2) is sufficient to determine the two identical x_σ , and in the following section we discuss how to obtain the two different x_σ in the presence of a magnetic field.

A. Magnetic susceptibility of FeSi

The simplest way to calculate the static susceptibility is to consider the one electron GFs in the presence of a small magnetic field in the z direction, and obtain $n_{f,\sigma}$, $n_{c,\sigma}$ by employing Eqs.(2.14-2.16) and the corresponding relations for the conduction electrons. The static magnetic susceptibility is then proportional to $g_f (n_{f,\downarrow} - n_{f,\uparrow}) + g_c (n_{c,\downarrow} - n_{c,\uparrow})$ when we neglect the Van Vleck contributions, and the calculation of the corresponding approximate GFs in the presence of a field is simpler when the gyromagnetic factors g_f and g_c of the two type of electrons are equal. The susceptibility $\chi(T)$ is then proportional to $n_\downarrow - n_\uparrow$ divided into the magnetic field, where $n_\sigma = n_{f,\sigma} + n_{c,\sigma}$ is the total number of electrons per site for each spin component σ . To calculate the two factors x_σ of the ‘‘ad hoc’’ renormalization we need of a further relation besides Eq.(3.2). We notice that each $G_{ff,\sigma}(\mathbf{k}, z)$ would give an independent $n_{f,0}$, and the two resulting values are in general different in the presence of the field, so we ask of them to be equal as the extra condition. The following symmetric equations are then obtained

$$\begin{aligned} x_\uparrow D_\uparrow + x_\downarrow n_\downarrow &= 1 \quad , \\ x_\downarrow D_\downarrow + x_\uparrow n_\uparrow &= 1 \quad , \end{aligned} \quad (3.3)$$

where $n_{f,\sigma}$ and D_σ are given in Eqs.(2.14,2.19).

To compare the ratio $\chi(T)/\chi(T_m)$ with the corresponding experimental value, it is necessary to chose the energy units to make the fit, and it was found that a convenient method was to start the calculations with the given unscaled $2W$ and E_f and a trial set of the remaining parameters, and then obtain the position T_m^{calc} of the calculated maximum of $\chi(T)$. The constant s_T defined by $T_m = 536 K = s_T T_m^{calc}$ would then give the required scaling, so that multiplying all the unscaled energy parameters times s_T , would give their absolute values in units of degree K . As the maximum of $\chi(T)$ is rather flat, it was found that a

better procedure was to find an s_T that would give the best fit of $\chi(T)/\chi(T_m)$ at moderately low T . All the adjustments were made by trial and error and direct comparison of the two curves in the plot

A very good fit was obtained by keeping a constant $\mu = 4.3$ with the $2W = 5\pi$ and $E_f = 4$, discussed above, and the relation $n_{tot} = 2.0$ was approximately satisfied at low T , but we could not find a similar set of parameters that would give a good fit for all the values of T when requiring a constant $n_{tot} = 2.0$. As the interval of temperatures is rather large, we considered that because of the lattice thermal expansion, some of the parameters could also change with T , and for simplicity we employed a linear change in the hybridization constant: $V(T) = V_0 (1 + \alpha_V T)$, where it is sufficient to leave all the scaling in V_0 and use always the unscaled α_V and T in the product $\alpha_V T$. A very good fit shown in figure 5 was then obtained with $V_0 = 1.8$ and $\alpha_V = -1.2$ and a position of the zero-width conduction band, employed to calculate $M_{2,\sigma}^{at}(z)$, given by $E_0^a = \mu - \delta E_0$ with a $\delta E_0 = 0.3$ independent of T . The scaling of the parameters was given by $s_T = 1750 \text{ K} \simeq 0.1508 \text{ eV}$, so that in absolute units $2W = 2.379 \text{ eV}$, $E_f = 603.2 \text{ meV}$, $V_0 = 271.4 \text{ meV}$ and $\delta E_0 = 45.24 \text{ meV}$.

We shall employ the same values of these parameters when comparing the theory with the measured resistivity in the following section, so that a consistent description of the two properties be obtained.

It is possible from our calculations to analyze the changes with T of the total occupations n_f and n_c of the f and c electrons respectively, and we have found that in the calculated curve of figure 5 the n_f changes from 0.47 at low T to 0.53 at 800 K. These parameter values show that the system remains in the intermediate valence region. It is also interesting to compare the separate contributions $\chi_f(T)$ and $\chi_c(T)$ of the f and c electrons to the total $\chi(T) = \chi_f(T) + \chi_c(T)$, and these two quantities are plotted in figure 6. Both follow the same trend of the total $\chi(T)$, but $\chi_c(T)$ is much smaller than $\chi_f(T)$, so that the choice of equal gyromagnetic factors for the two type of electrons should not affect the final result in a substantial way.

B. Resistivity of FeSi

The dynamic conductivity $\sigma(\omega, T)$ is related to the current current correlations by the well known Kubo formula.^{62,63} Two-particle GF are then necessary to calculate those correlations, and to simplify the calculations, Schweitzer and Czycholl²⁶ employed the expression of the conductivity for dimension $d = \infty$ as an approximation of the static conductivity for $d = 3$. Only one-particle GFs are then necessary to obtain $\sigma(\omega, T)$ in that limit, because the vertex corrections cancel out,²⁷ and we shall follow the same approach. As the hybridization is a hopping of electrons between two different bands, it contributes to the current operator in the PAM,⁶⁴ but this contribution cancels out in our model because we employ a local hybridization $V_{j,\mathbf{k},\sigma} = V_{j,\sigma}$. The expression obtained contains explicit sums over \mathbf{k} , but it is possible to make a further simplification by considering nearest-neighbor hopping in a simple cubic lattice,^{28,29,65} and the sums over \mathbf{k} can be transformed²³ in integrals over the free conduction electron energy $\varepsilon(\mathbf{k})$. This transformation is possible because in the AECA the $G_{cc,\sigma}(\mathbf{k}, \omega)$ is a function of \mathbf{k} only through the $\varepsilon(\mathbf{k}) = \varepsilon$, as both $M_{2,\sigma}^{at}(z)$ and $V_{j,\mathbf{k},\sigma} = V_{j,\sigma}$ are \mathbf{k} independent. We can then write

$$\rho_{c,\sigma}(\omega; \varepsilon) = \frac{1}{\pi} \lim_{\eta \rightarrow 0} \text{Im} \{G_{cc,\sigma}(\mathbf{k}, \omega + i|\eta|)\} \quad , \quad (3.4)$$

and the dynamical conductivity is given by

$$\sigma(\omega, T) = C_0 \frac{1}{\omega} \int_{-\infty}^{\infty} d\omega' [f_T(\omega') - f_T(\omega' + \omega)] \int_{-\infty}^{\infty} d\varepsilon \rho_{c,\sigma}(\omega'; \varepsilon) \rho_{c,\sigma}(\omega' + \omega; \varepsilon) \varrho_{\sigma}^0(\varepsilon) \quad , \quad (3.5)$$

where C_0 is a constant discussed below and $\varrho_{\sigma}^0(\varepsilon)$ is the density of states of the free conduction electrons per site and per spin.

The static conductivity is then given by

$$\sigma(T) = C_0 \int_{-\infty}^{\infty} d\omega \left(- \frac{df_T(\omega)}{d\omega} \right) S(\omega) \quad , \quad (3.6)$$

where

$$S(\omega) = \int_{-\infty}^{\infty} d\varepsilon (\rho_{c,\sigma}(\omega; \varepsilon))^2 \varrho_{\sigma}^0(\varepsilon) \quad . \quad (3.7)$$

The constant

$$C_0 = \pi \frac{e^2}{\hbar} \frac{1}{a} \frac{2}{d} t^2 \quad , \quad (3.8)$$

where a is the lattice parameter of FeSi and t is the hopping parameter of the hypercubic lattice that gives the c electron energy²³

$$\varepsilon(\mathbf{k}) = - \left(\frac{2t}{\sqrt{2d}} \right) \sum_{\nu=1}^d \cos(a k_{\nu}) \quad . \quad (3.9)$$

We shall generally use a rectangular band with $-W \leq \varepsilon(\mathbf{k}) \leq W$, and to relate t to W we consider that the band width $\sqrt{2d} 2t$ of Eq. (3.9) should be equal to $2W$, so that $t = W/\sqrt{2d}$. Replacing $d = 3$, $2W = 5\pi$ and $a = 4.489\text{\AA}^5$ in Eq. (3.8) we find⁶⁶ $C_0 = 6180/(\Omega \text{ cm})$.

If in the AECA of Eq. (2.21) we abbreviate $G_{cc,\sigma}(\mathbf{k}, z) = -[a - \varepsilon(\mathbf{k}) + i b]^{-1}$, with real a and b (functions of ω) defined by $a + i b = z + |V|^2 M_{2,\sigma}^{at}(z)$, we find that when $b \rightarrow 0$ then $S(\omega) \sim O|1/b|$ if ω is outside the gap and $S(\omega) \sim O|b^2|$ if ω is inside. This different behaviors can give rather different low T limits of $\sigma(T)$, because the integrand in Eq.(3.6) only contributes in an interval of $O|T|$ around the Fermi energy $\omega = 0$ (our frequency variables are given with respect to μ). When $\omega = 0$ is inside the gap we then have a very small $\sigma(0)$ if $\text{Im} M_{2,\sigma}^{at}(0) \sim 0$, which corresponds to the case of FeSi at low T , as is discussed below.

To analyze $M_{2,\sigma}^{at}(z)$ we notice from Eq. (2.26) that $G_{ff,0\sigma}^{at}(z)$ is real when $\eta \equiv \text{Im}[z] \rightarrow 0$, except at its only singularities on the real axis, that are the poles at $z = u_j$. It is then clear from Eq. (2.27) that $M_{2,\sigma}^{at}(z)$ is real on the real axis of the z complex plane,⁶⁷ except at the real solutions of $(\omega - E_0^a + \mu) - |V|^2 G_{ff,0\sigma}^{at}(\omega) = 0$, where it would have poles with

$Im M_{2,\sigma}^{at}(z) \neq 0$ in their neighborhood. One should then make all the calculations at a finite η and afterwards take $\eta \rightarrow 0$.

In figure 7 we plot the local spectral density of the conduction electrons, namely

$$\rho_{c,\sigma}(\omega) = \frac{1}{\pi} \lim_{\eta \rightarrow 0} Im \left\{ \frac{1}{N_s} \sum_{\mathbf{k}} G_{cc,\sigma}(\mathbf{k}, \omega + i |\eta|) \right\} \quad (3.10)$$

as well as $Im M_{2,\sigma}^{at}(\omega + i |\eta|)$ as a function of ω for the same parameters employed in figure 5, but in this plot the variable ω , as well as the fixed parameters $T = 0.001$ and $\eta = 0.00001$, are given in the unscaled energy units. It is clear from figure 7 that for these η and T the peaks of $Im M_{2,\sigma}^{at}(\omega + i |\eta|)$ are very sharp, and that the region where this quantity is appreciably large is far away from $\omega = 0$ in units of T . The value of the b defined above is therefore very small at that $\omega = 0$, and the conductivity would be extremely low because that value of ω is well inside the gap so that $S(\omega) \sim O |b^2|$. If the Fermi surface ($\omega = 0$) were inside the conduction band, the $S(\omega) \sim O |1/b|$ and the conductivity would be extremely large, and would tend to infinity when $\eta \rightarrow 0$. The physical reason for this different behaviors at very low T is the absence of carriers when $\omega = 0$ is inside the gap, and the absence of scattering mechanisms for the c-electrons when $\omega = 0$ is inside the band.

The extreme sharpness of the structure of $Im M_{2,\sigma}^{at}(z)$ is a consequence of the atomic approximation employed, and to alleviate this character we have added an extra imaginary part $\eta_a = |\eta_a| \text{sgn}(Im[z])$ to its argument : $M_{2,\sigma}^{at}(z) \implies M_{2,\sigma}^{at}(\omega + i\eta_a)$, so that the poles of this quantity become Lorentzians that somehow mimic the effect of the band width. To show the effect of this change, the plot of $Im M_{2,\sigma}^{at}(z)$ is also shown in figure 7 for the same parameters used above but for an unscaled $\eta + \eta_a = 0.001$. The $Im M_{2,\sigma}^{at}(z)$ has now an appreciable value at $\omega = 0$ and reaches inside the conduction band, and $\sigma(T)$ is much larger than before, but it is still rather small because T is small and only an interval of order of T contributes to $\sigma(T)$.

Addition of η_a to the argument of $M_{2,\sigma}^{at}(z)$ leads to similar effects as those already obtained by Mutou and Hirashima²⁸ through ‘‘introducing a small imaginary part Γ to the conduction electrons’’, i.e. replacing $z = i \omega$ by $z + i \Gamma \text{sgn}(\omega)$ in the GFs $G_{ff,\sigma}(\mathbf{k}, z)$ and $G_{cc,\sigma}(\mathbf{k}, z)$. Their justification is the existence in real systems of scattering processes due to phonons and impurities, and we should also consider this mechanisms as contributing to the $i\eta_a$. Within this interpretation one could also consider a temperature dependence of η_a , but we have not implemented this change in the present calculation.

It seems clear that the basic scattering mechanism in our calculation of the PAM’s $\sigma(T)$ is the hybridization, because the otherwise free conduction electrons are scattered by the localized f electrons through this interaction. This is apparent if we notice that the relaxation effects are described by the imaginary part of the usual self-energy $\Sigma_{cc,\sigma}(\mathbf{k}, z)$, defined through

$$G_{cc,\sigma}(\mathbf{k}, z) = - \{z - \varepsilon(\mathbf{k}) - \Sigma_{cc,\sigma}(\mathbf{k}, z)\}^{-1} \quad , \quad (3.11)$$

and that the exact relation $\Sigma_{cc,\sigma}(\mathbf{k}, z) = - |V(\mathbf{k})|^2 M_{2,\sigma}^{eff}(\mathbf{k}, z)$ follows from Eq. (2.21). The relaxation mechanism of the c-electrons is then provided by the hybridization, and the self energy is independent of \mathbf{k} in the AECA: $\Sigma_{cc,\sigma}(z) = - |V|^2 M_{2,\sigma}^{at}(z)$.

As discussed above, the vanishing resistivity obtained in our approximation when μ is inside the conduction band and $T \rightarrow 0$ is caused by the atomic character of our effective cumulant $M_{2,\sigma}^{at}$, and the introduction of a finite η_a moderates this effect. In our calculation of $\rho(T) = 1/\sigma(T)$ we have chosen η_a to obtain a reasonable agreement with the measured values for T above 50 K, because the conduction by ionized impurities would dominate $\sigma(T)$ at lower temperatures.⁶⁸ In figure 8 we plot $\rho(T)$ for the same parameters employed to calculate $\chi(T)$ in figure 5, but for an unscaled $\eta_a = 0.0008$. The plot is compared to the experimental values measured² by Schlesinger et.al., which we obtained by digitalization of their plot. We have preferred these values to those of other authors^{69,70} because the higher values of $\rho(T)$ seem to indicate a better sample with less impurities. The agreement is fairly good above 50 K, and the much lower experimental resistivity below this T is attributed to the ionic conduction, as mentioned above. The impurity scattering is T independent and could be considered to be included in the value of η_a we used, but the phonon scattering would increase with T , and one should start with a smaller η_a and add a contribution that has the T dependence corresponding to this process. This effect could explain the difference between the two curves above $T = 200$ K.

We point out that the typical values of η_a we have used would not affect the values of $\chi(T)$, although they were essential in fitting $\rho(T)$ to the experimental values.

IV. CONCLUSIONS

In this work we have used approximate⁹ one-electron GFs of the PAM in the limit $U \rightarrow \infty$ to study the static magnetic susceptibility $\chi(T)$ and electrical resistivity $\rho(T)$ of FeSi, which has the typical behavior of the Kondo insulators. The total number of electrons per site $n_{tot} = 2$ we have selected seems a good choice for FeSi, and at each T it is then necessary to find the value of the chemical potential μ that gives this n_{tot} .

The exact GFs of the PAM are formally derived from their cumulant expansion,¹⁸ and are expressed in terms of an effective cumulant $M_{2,\sigma}^{eff}(\mathbf{k}, z)$, that is given by the contribution of all the proper diagrams of the exact GF $G_{ff,\sigma}(\mathbf{k}, z)$. To obtain approximate GFs, we substitute $M_{2,\sigma}^{eff}(\mathbf{k}, z)$, whose calculation is as difficult as that of $G_{ff,\sigma}(\mathbf{k}, z)$, by the corresponding quantity of an exactly soluble model, which is the same PAM but with a conduction band of zero width. The use of this atomic limit makes the corresponding effective cumulant $M_{2,\sigma}^{at}(z)$ independent of \mathbf{k} , and the approximate GFs have the same structure obtained by the dynamical mean field theory.²¹ While this last method uses self-consistency conditions to obtain the final GFs, we use physical considerations to chose the parameters that define $M_{2,\sigma}^{at}(z)$. The approximation we employ does not give results as accurate as that theory, but has the advantage that the numerical calculation is fairly rapid, and that it can be extended to more complex systems with a large number of local states, by projecting the large space of these states into a manageable subspace of interest with the use of Hubbard operators.

We have shown that the spectral density ρ_f of the approximate GF employed in this work has, at low T and in the Kondo region, a structure on the Fermi surface that can be interpreted as the Kondo peak, a feature that was missing in our cumulant expansions when only cumulants up to fourth order were employed.¹⁸ This behavior is essential for the calculation of the system's properties, and as the spectral densities obtained by the AECA

have the overall behavior that is expected from the model,⁴⁰ the use of this approximation would then be expected to give, without too heavy computation, rather reasonable values of many physical properties and of their dependence with T and other parameters.

These approximate one-electron GFs of the PAM in the limit $U \rightarrow \infty$, are used here to describe the static magnetic susceptibility $\chi(T)$ and electrical resistivity $\rho(T)$ of FeSi, a compound which has the typical behavior of the Kondo insulators. We have selected a total number of electrons per site $n_{tot} = 2$, because it seems a good choice for FeSi, and at each T it was then necessary to find the value of the chemical potential μ that gives this n_{tot} . We tried to describe the system employing a typical intermediate valence situation, and this was achieved with a rectangular band of total width $2W = 5\pi$ and an unperturbed energy $E_f = 4$. of the f-electrons, requiring a chemical potential $\mu \sim 4$ to satisfy $n_{tot} = 2$. These unscaled values correspond to measuring the energy parameters in units of $2W/5\pi$.

The susceptibility $\chi(T)$ is proportional to the difference $n_{\downarrow} - n_{\uparrow}$ between the occupation number of up and down electrons, and we have fitted the calculated $\chi(T)/\chi(T_m)$ to the experimental results,¹ where $\chi(T_m)$ is the maximum value of the susceptibility. We have found that the contribution of the conduction electrons to $\chi(T)$ is much smaller than that of the local electrons for the employed parameters (cf. figure 6), and the assumption made of equal gyromagnetic factors for the two type of electrons has therefore no major relevance.

To find the factor s_T that transforms the unscaled parameters into absolute units, we have scaled the calculated $\chi(T)/\chi(T_m)$ curve so that it agrees with the experimental one at low T . It was not possible to find a set of parameters that would give a good agreement at both low and high T , and we considered that because of thermal expansion some of the parameters could change with T . Assuming a linear dependence $V(T) = V_0 (1 + \alpha_V T)$ of the hybridization parameter V it was then possible to obtain a rather good agreement in the whole T range (cf. figure 5). Although this is a very crude model of these effects and one should also expect changes of E_f , it shows that the dependence of the model's parameters with thermal expansion should not be neglected.

To calculate $\rho(T)$ we used an expression valid for infinite dimension,²⁶ and assumed a nearest neighbor hopping in a simple cubic lattice to transform the sums over \mathbf{k} into integrals over the unperturbed energies $\varepsilon(\mathbf{k})$ of the conduction electrons. As a further non-essential simplification we used a rectangular band for the corresponding spectral density ϱ_{σ}^0 .

We have shown that the relaxation mechanism of the c-electrons is provided by the hybridization, and the most likely situation in the AECA is that the conductivity vanishes as $T \rightarrow 0$ when μ is inside the gap and tends to infinity when μ is inside the band. Here we show that this result is a consequence of the atomic character of the AECA, that makes $M_{2,\sigma}^{at}(z)$ imaginary only in the neighborhood of its finite number of poles that are usually far apart from the Fermi surface ($\omega = 0$). This behavior is moderated by introducing an extra imaginary part η_a to its argument (cf. figure 7), whose effect is similar to that of scattering of the c-electrons by phonons and impurities.²⁸ The resistivity at low temperatures is probably determined by ionic conduction, and if we choose η_a so that the calculated resistivity coincides with the experimental one close to $T \sim 50K$, a very good agreement is obtained up to $T \sim 200K$. The departures at higher T could be attributed to the phonon scattering.

In summary, we have shown that the spectral densities obtained by the AECA have the overall behavior that is expected from the PAM, and we can therefore expect that

this approximation would give, without too heavy computation, rather reasonable values of many physical properties and of their dependence with T and other parameters. We have employed the AECA to study FeSi assuming a typical intermediate valence situation of the PAM in the $U \rightarrow \infty$ limit, and we were able to give a good description of both the static resistivity and magnetic susceptibility of FeSi as a function of T employing a single set of the model's parameters.

V. ACKNOWLEDGEMENTS

The authors are grateful to Profs. Roberto Luzzi, Marcelo J. Rozenberg, Mucio A. Continentino and Sergio S. Makler for critical comments. They would like to acknowledge financial support from the following agencies: CNPq (MSF), FAPESP and CNPq (MEF). This work was done (in part) in the frame of Associate Membership Programme of the International Centre for Theoretical Physics, Trieste ITALY (MEF).

REFERENCES

- ¹ V. Jacarino, G. K. Wertheim, J. H. Wernick, L. R. Walder and S. Araj, Phys. Rev. **160**, 476 (1967)
- ² Z. Schlesinger, Z. Fisk, Hai-Tai Zhang, M. B. Maple, J. F. DiTusa and G. Aeppli, Phys. Rev. Lett. **71**, 1748 (1993)
- ³ G. Aeppli and Z. Fisk, Comment. Cond. Mat. Phys. **16**, 155 (1992)
- ⁴ Z. Schlesinger, Z. Fisk, Hai-Tai Zhang, M. B. Maple, Physica B, **237-238**, 460 (1997)
- ⁵ L. Mattheiss and D. Hamann, Phys. Rev. B **47**, 13114 (1993)
- ⁶ C. Fu and S. Doniach, Phys. Rev. B **51**, 17439 (1995)
- ⁷ M. A. Continentino, G. M. Japiassu and A. Troper, Phys. Rev. B **49**, 4432 (1994)
- ⁸ M. V. Tovar Costa, A. Troper, N. A. de Oliveira, G. M. Japiassu and M. A. Continentino Phys. Rev. B **57**, 6943 (1998)
- ⁹ M. E. Foglio, Brazilian Journal of Physics, **27**, 644 (1997)
- ¹⁰ C. Sanchez-Castro, K. S. Bedell and B. R. Cooper, Phys. Rev. B **47**, 6879 (1993)
- ¹¹ P. S. Riseborough, Phys. Rev. B **45**, 13984 (1992)
- ¹² C. M. Varma, Phys. Rev. B **50**, 9952 (1994)
- ¹³ Varma¹² argues that the absence of low energy magnetic correlations, as observed in strongly correlated insulators, is characteristic of the mixed valent character of these insulators. This could be related to the lack of magnetic interactions between low energy quasiparticles observed by neutron scattering experiments in FeSi.^{3,71}
- ¹⁴ J. Hubbard, Proc. R. Soc. London, Ser. A **285**, 542 (1965)
- ¹⁵ S. B. Haley and P. Erdos, Phys. Rev. B **5**, 1106 (1972)
- ¹⁶ J. Hubbard, Proc. R. Soc. London, Ser. A **276**, 238 (1964)
J. Hubbard, Proc. R. Soc. London, Ser. A **277**, 237 (1964)
J. Hubbard, Proc. R. Soc. London, Ser. A **281**, 401 (1964) (these are the first three papers of a series of six)
- ¹⁷ J. Hubbard, Proc. R. Soc. London, Ser. A **296**, 82 (1966)
- ¹⁸ M. S. Figueira, M. E. Foglio and G. G. Martinez, Phys. Rev. B **50**, 17933 (1994)
- ¹⁹ W. Metzner, Phys. Rev. B **43**, 8549 (1991)
- ²⁰ M. S. Figueira, *Doctoral Thesis* (Campinas, SP, Brasil: Universidade Estadual de Campinas, 1994)
- ²¹ A. Georges, G. Kotliar, W. Krauth and M. J. Rozenberg, Rev. Mod. Phys. **68**, 13 (1996)
- ²² W. Metzner and D. Vollhardt, Phys. Rev. Lett. **62**, 324 (1989)
- ²³ E. Muller Hartmann, Z. Phys. B **74**, 507 (1989)
- ²⁴ M. J. Rozenberg, Phys. Rev. B **52**, 7369 (1995)
- ²⁵ M. J. Rozenberg, G. Kotliar and H. Kajueter, Phys. Rev. B **54**, 8452 (1996)
- ²⁶ H. Schweitzer and G. Czycholl, Phys. Rev. Lett. **67**, 3724 (1991)
- ²⁷ A. Khurana, Phys. Rev. Lett. **64**, 1990 (1990)
- ²⁸ T. Mutou and D. S. Hirashima, J. Phys. Soc. Japan **63**, 4475 (1994)
- ²⁹ Th. Pruschke, D. L. Cox and M. Jarrell, Phys. Rev. B **47**, 3553 (1993)
- ³⁰ A. L. Fetter and J. D. Walecka, *Quantum Theory of Many-Particle Systems* (McGraw-Hill, New York, 1971).
- ³¹ It is clear that the two sides of Eq. (2.5) give the same result when applied to the basis $\{|j, 0\rangle, |j, \downarrow\rangle, |j, \uparrow\rangle, |j, 2\rangle\}$ of the space of local states at site j .

- ³² M. Wortis, in *Phase Transitions and Critical Phenomena*, edited by C. Domb and M. S. Green (Academic, London, 1974), Vol. **3**, pg.113.
- ³³ R. Kubo, J. Phys. Soc. (Jpn.) **17**, 1100 (1962)
- ³⁴ M. S. Figueira and M. E. Foglio, J. Phys.: Condens. Matter **8**, 5017 (1996)
- ³⁵ A. C. Hewson, J. Phys. C: Solid State Phys. **10**, 4973 (1977)
- ³⁶ D. H. Y. Yang and Y. L. Wang, Phys. Rev. B **10**, 4714 (1975)
- ³⁷ M. S. Figueira and M. E. Foglio, J. Phys.: Condens. Matter **8**, 5017 (1996)
- ³⁸ J. W. Negele and H. Orland *Quantum Many-Particle Systems* (Addison-Wesley, New York, 1988), Chap. 2.
- ³⁹ D. N. Zubarev, Usp. Fiz. Nauk. **71**, 71 (1960) [Sov. Phys.-Usp. **3**, 320 (1960)]
- ⁴⁰ A. C. Hewson, *The Kondo problem to Heavy Fermions* (Cambridge U.P. Cambridge, 1993)
P. Schlottmann, Phys.Rep. **181**, 1 (1989)
P. Fulde, Solid State Physics **41**, 1 (1988)
P. A. Lee, T. M. Rice, J. W. Serene, L. J. Sham and J. W. Wilkins, Comments Cond. Mat. Phys. **12**, 99 (1986).
- ⁴¹ J. Kondo, Progr. Theor. Phys. **32**, 37 (1964)
J. Kondo, Solid State Physics **23**, 184 (1969)
- ⁴² But note that the meaning of vertices and edges is exchanged with that employed in the cumulant expansion.
- ⁴³ J. M. Luttinger and J. C. Ward, Phys. Rev. **118**, 1417 (1960)
- ⁴⁴ L. Craco and M. A. Gusmão, Phys. Rev. B **54**, 1629 (1996)
- ⁴⁵ M. E. Foglio and M. S. Figueira, J. Phys. A Mathematics and General **30** 7879 (1997)
- ⁴⁶ See Appendix A of Fulde's review and Appendix C of Hewson's review, cited in reference 40.
- ⁴⁷ M. E. Foglio and L. M. Falicov, Phys. Rev. B **20**, 4554 (1979)
- ⁴⁸ M. E. Foglio, C. A. Balseiro and L. M. Falicov, Phys. Rev. B **20**, 4560 (1979)
- ⁴⁹ B. Alascio, R. Allub and A. A. Aligia, Z. Phys. B **36**, 37 (1979)
- ⁵⁰ A. Alascio, R. Allub and A. A. Aligia, J. Phys. C: Solid State Phys. **13**, 2869 (1980)
- ⁵¹ A. S. R. Simões, J. R. Iglesias and E. V. Anda, Phys. Rev. B **29**, 3085 (1984)
- ⁵² E. V. Anda, J. Phys. C: Solid State Phys. **14**, L1037 (1981)
- ⁵³ A. S. R. Simões, J. R. Iglesias, A. Rojo and B. Alascio, J. Phys. C: Solid State Phys. **21**, 1941 (1988)
- ⁵⁴ A. S. R. Simões, *Doctoral Thesis* (Porto Alegre, RS, Brasil: Universidade Federal de Rio Grande do Sul, 1986)
- ⁵⁵ L. G. Brunet, R. Ribeiro-Teixeira and J. R. Iglesias, Sol. Stat. Comm. **68**, 477 (1988)
- ⁵⁶ L. G. Brunet, M. A. Gusmão and J. R. Iglesias, Phys. Rev. B **46**, 4520 (1992)
- ⁵⁷ R. Consiglio, *Doctoral Thesis* (Porto Alegre, RS, Brasil: Universidade Federal do Rio Grande do Sul, 1997)
- ⁵⁸ G. G. Martinez Pino, *Doctoral Thesis* (Campinas, SP, Brasil: Universidade Estadual de Campinas, 1989).
- ⁵⁹ H. Kaga, H. Kubo and T. Fujiwara, Phys. Rev. B **37**, 341 (1988)
- ⁶⁰ N. Grewe, Sol. Stat. Comm. **50**, 19 (1984)
- ⁶¹ M. S. Figueira and M. E. Foglio, Int. J. Mod. Phys. B **12**, 837 (1998)
- ⁶² R. Kubo, J. Phys. Soc. Japan **12**, 570 (1957)
- ⁶³ G. D. Mahan *Many-Particle Physics* (Plenum Press, New York, 1990).

- ⁶⁴ G. Czycholl and H. J. Leder, Z. Phys. B **44**, 59 (1981)
- ⁶⁵ R. Consiglio and M. A. Gusmão, Phys. Rev. B **55**, 6825 (1997)
- ⁶⁶ The $G_{cc,\sigma}(\mathbf{k}, \omega)$ and $\rho_{c,\sigma}(\omega; \varepsilon)$ employed in Eq. (3.6) are calculated with the unscaled values of all the parameters, and in the calculation of C_0 one should then use the same type of units for t^2 .
- ⁶⁷ The real value $M_{2,\sigma}^{at}(u_j) = - (u_j - E_0^a + \mu) / |V|^2$ is taken at the poles u_j of $G_{ff,0\sigma}^{at}(z)$.
- ⁶⁸ D. Mandrus, J. L. Sarrao, A. Migliori, J. D. Thompson and Z. Fisk, Phys. Rev. B **51**, 4763 (1995)
- ⁶⁹ B. C. Sales, E. C. Jones, B. C. Chakoumakos, J. A. Fernandez-Baca, H. E. Harmon and J. W. Sharp, Phys. Rev. B **50**, 8207 (1994)
- ⁷⁰ M. B. Hunt, M. A. Chernikov, E. Felder and H. R. Ott Phys. Rev. B **50**, 14933 (1994)
- ⁷¹ K. Tajima, Y. Endoh, J. E. Fischer and G. Shirane, Phys. Rev. B **44**, 6954 (1988)

FIGURES

FIG. 1. Typical cumulant diagrams for one-particle GF, where the filled and empty circles represent the f-electron and c-electron free propagators respectively, and the lines joining them represent the hybridization interaction. (a) The diagrams of the chain approximation (CHA) for the f-electrons, represented by the filled square to the right. (b) As (a) but for the c-electrons, represented by an empty square. (c) A more complicated diagram, with cumulants of fourth and sixth order.

FIG. 2. The energies $\varepsilon_{n,r} = E_{n,r} - n\mu$ of the twelve eigenstates $|n, r\rangle$ of the atomic limit are represented in this figure, and those corresponding to different occupations $n = 0, 1, 2, 3$ are drawn in different columns. The index r that characterizes the states is written above the corresponding levels, and the lines joining different levels are identified by numbers i , showing the possible transitions u_i that contribute to the GF. As with Eqs. (2.8,2.9), the frequencies have the chemical potential μ subtracted, so that the Fermi surface corresponds to $\omega = 0$.

FIG. 3. The spectral density $\rho_f(\omega)$ of the f-electrons obtained with the AECA for several values of T , employing $z = \omega + i\eta$ with $\eta = 10^{-4}$. The system has the following parameters: $E_f = -0.5$, $\mu = 0.$, $T = 0.001$, a local hybridization $V = 0.3$ and a density of states of the unperturbed band electrons given by a rectangular density of states of width π centered at the origin, all in the same energy units. The effective cumulant was calculated employing a reduced hybridization $V_a = \Delta = V^2$ and a frequency with a small imaginary part $\eta_a = 0.003$ (further details of the introduction of η_a are given in Subsection III B).

FIG. 4. The spectral density of the f-electrons for the same system of figure 3 but with fixed $T = 0.001$ and for several values of the chemical potential μ . It shows the crossover from the Kondo region to the intermediate valence region.

FIG. 5. The reduced susceptibility $\chi(T)/\chi(T_m)$ as a function of T , where $\chi(T_m)$ is the maximum value of $\chi(T)$. The open circles correspond to the experimental values, taken from reference 1. The full line corresponds to the model's calculation for a rectangular band with a total width $2W = 5\pi$, an f electron energy of $E_f = 4.$, a total number of electrons $n_{tot} = 2.0$, a T dependent hybridization $V(T) = 1.8(1. - 1.2T)$ and the zero-width conduction band employed in the model located at $E_0^a = \mu - \delta E_0$ with a T -independent $\delta E_0 = 0.3$. These unscaled values have to be multiplied by the scale factor $s_T = 1750 K = 150.8$ meV to express them in absolute units: $2W \simeq 2.379$ eV, $E_f = 603.2$ meV, $V_0 = 271.4$ meV and $\delta E_0 = 45.24$ meV.

FIG. 6. The separate susceptibilities $\chi_f(T)$ (full line) and $\chi_c(T)$ (dotted line) of the f and c electrons respectively, as a function of T and for the same parameters of figure 5.


FIG. 7. The spectral density of the conduction electrons $\rho_{c,\sigma}(\omega)$ times π (full line) and the imaginary part of the approximate effective cumulant $M_{2,\sigma}^{at}(z)$ (dotted and dash-dotted lines) are plotted in a logarithmic scale as a function of ω for $T = 0.001$, $\eta = 0.00001$, $\eta_a = 0$. (full and dotted line), $\eta + \eta_a = 0.001$ (dash-dotted line) and the same parameters of figure 5. The values of ω , T , η and η_a are given in unscaled energy units, and have to be multiplied by the scale factor $s_T = 1750 \text{ K} = 150.8 \text{ meV}$ to express them in absolute units.

FIG. 8. The resistivity $\rho(T)$ in $\Omega \text{ cm}$, measured by Schlesinger et al.² (triangles) and calculated (full line) with Eq. (3.6) and the same parameters employed in figure 5, but with $\eta_a = 0.0008$. The values of ω and η are given in unscaled units, and have to be multiplied by the scale factor $s_T = 1750 \text{ K} = 150.8 \text{ meV}$ to express them in absolute units.

TABLES

n	r	S_z	$\varepsilon_{n,r} = E_{n,r} - n\mu$
0	1	0	E_0
1	2	$+\frac{1}{2}$	$\frac{1}{2} \left(E_0 + E_f - \sqrt{(E_0 + E_f)^2 + 4V^2} \right) - \mu$
1	3	$-\frac{1}{2}$	$\frac{1}{2} \left(E_0 + E_f - \sqrt{(E_0 + E_f)^2 + 4V^2} \right) - \mu$
1	4	$+\frac{1}{2}$	$\frac{1}{2} \left(E_0 + E_f + \sqrt{(E_0 + E_f)^2 + 4V^2} \right) - \mu$
1	5	$-\frac{1}{2}$	$\frac{1}{2} \left(E_0 + E_f + \sqrt{(E_0 + E_f)^2 + 4V^2} \right) - \mu$
2	6	+1	$E_0 + E_f - 2\mu$
2	7	-1	$E_0 + E_f - 2\mu$
2	8	0	$E_0 + E_f - 2\mu$
2	9	0	$\frac{1}{2} \left(E_0 + 3E_f - \sqrt{(E_0 + E_f)^2 + 8V^2} \right) - 2\mu$
2	10	0	$\frac{1}{2} \left(E_0 + 3E_f + \sqrt{(E_0 + E_f)^2 + 8V^2} \right) - 2\mu$
3	11	$+\frac{1}{2}$	$E_0 + 2E_f - 3\mu$
3	12	$-\frac{1}{2}$	$E_0 + 2E_f - 3\mu$

TABLE I. The properties of the twelve eigenstates $|n, r\rangle$ of \mathcal{H} are given. The columns are labeled by the number of electrons n , the name r of the state, the z spin component S_z of the state and the value of $\varepsilon_{n,r} = E_{n,r} - n\mu$, where $E_{n,r}$ is the energy of the state $|n, r\rangle$.

a) 

b) 

